AD-A124 098 EXPLORATION OF THE FEASIBILITY OF PRESENT GENERATION 1/
LITHIUM BATTERIES FOR ELECTRIC VEHICLES(U) EIC LABS INC
NEWTON MA P B HARRIS ET AL. NOV 82 C-480A
UNCLASSIFIED N00014-77-C-0155 F/G 10/3 NL

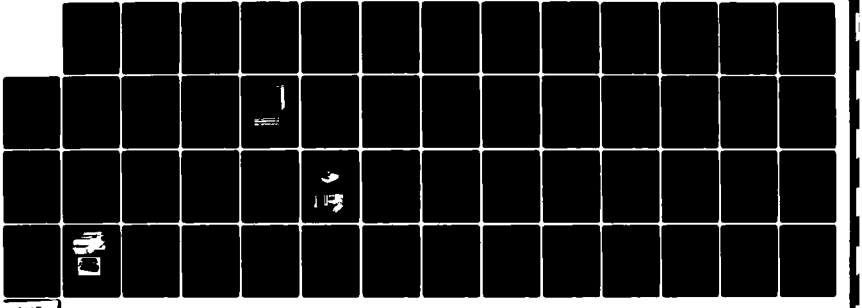

END
DATE FILMED
2-83
DTIC

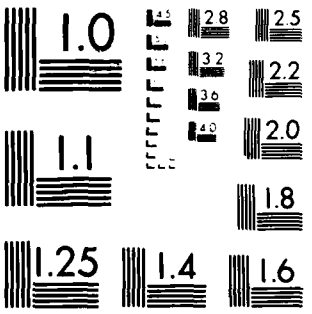

12

OFFICE OF NAVAL RESEARCH

Contract No. N00014-77-C-0155

Task No. NR 359-638

TECHNICAL REPORT NO. 9

EXPLORATION OF THE FEASIBILITY OF PRESENT GENERATION LITHIUM BATTERIES FOR ELECTRIC VEHICLES

by

P. B. Harris, G. L. Holleck, J. Buzby, J. Avery,
L. Pitts and K. M. Abraham

EIC Laboratories, Inc.
67 Chapel Street
Newton, Massachusetts 02158

November 1982

This project was supported in part by the Office of Naval Research and by the Department of Energy, Washington, D.C. The Department of Energy Work was carried out via a subcontract through Naval Ocean Systems Center, San Diego, CA. The subcontract monitor was Joseph McCartney.

UNCLASSIFIED

SECURITY CLASSIFICATION OF THIS PAGE (When Data Entered)

REPORT DOCUMENTATION PAGE		READ INSTRUCTIONS BEFORE COMPLETING FORM
1. REPORT NUMBER TECHNICAL REPORT NO. 9	2. GOVT ACCESSION NO. AD-A124 098	3. RECIPIENT'S CATALOG NUMBER
4. TITLE (and Subtitle) EXPLORATION OF THE FEASIBILITY OF PRESENT GENERATION LITHIUM BATTERIES FOR ELECTRIC VEHICLES		5. TYPE OF REPORT & PERIOD COVERED Technical Report 6. PERFORMING ORG. REPORT NUMBER C480A
7. AUTHOR(s) P. B. Harris, G. L. Holleck, J. Buzby, J. Avery, L. Pitts, and K. M. Abraham		8. CONTRACT OR GRANT NUMBER(s) N00014-77-C-0155
9. PERFORMING ORGANIZATION NAME AND ADDRESS EIC Laboratories, Inc. 67 Chapel Street Newton, Massachusetts 02158		10. PROGRAM ELEMENT, PROJECT, TASK AREA & WORK UNIT NUMBERS NR 359-638
11. CONTROLLING OFFICE NAME AND ADDRESS Office of Naval Research/Chemistry Program Arlington, Virginia 22217		12. REPORT DATE November 1982 13. NUMBER OF PAGES 41
14. MONITORING AGENCY NAME & ADDRESS(if different from Controlling Office)		15. SECURITY CLASS. (of this report) UNCLASSIFIED 15a. DECLASSIFICATION/DOWNGRADING SCHEDULE

16. DISTRIBUTION STATEMENT (of this Report)

Approved for Public Release; Distribution Unlimited.

17. DISTRIBUTION STATEMENT (of the abstract entered in Block 20, if different from Report)

18. SUPPLEMENTARY NOTES

19. KEY WORDS (Continue on reverse side if necessary and identify by block number)

Ambient temperature rechargeable lithium cells, Molybdenum trisulfide cathodes, 2Methyl-tetrahydrofuran/$LiAsF_6$ electrolytes for cycling lithium, Use of ambient temperature lithium cells for electric vehicles.

20. ABSTRACT (Continue on reverse side if necessary and identify by block number)

The present technology of secondary Li batteries was investigated with regard to feasibility for use in automotive propulsion systems. A computer modeling effort examined series vs. parallel plate arrangement in battery modules and critical factors limiting energy density in each case. It was found that the most critical factor is the cathode energy density, and that to achieve the ultimate goal of 125 Wh/lb (275 Wh/kg) a cathode energy density of 290 Wh/lb (630 Wh/kg) is necessary. 20 Ah

DD FORM 1 JAN 73 1473 EDITION OF 1 NOV 65 IS OBSOLETE

UNCLASSIFIED

SECURITY CLASSIFICATION OF THIS PAGE (When Data Entered)

$Li/LiAsF_6$ in 2Me-THF/MoS_3 cells were built and tested. Cycle regimes and results are discussed. Although MoS_3 is theoretically capable of providing the necessary energy density to meet the ultimate goal, it requires more development to overcome chemical instability in the system. At present none of the cathode materials examined - TiS_2, V_6O_{13} and MoS_3 - is capable of satisfying the energy density goal.

TABLE OF CONTENTS

TABLE OF CONTENTS
(continued)

LIST OF ILLUSTRATIONS

LIST OF TABLES

1.0 INTRODUCTION

This project was concerned to make a preliminary exploration of the feasibility for using present generation, ambient temperature rechargeable Li battery technology to power electric vehicles. The program was originally intended to be carried out over two years but due to funding limitations at the Department of Energy it was not continued beyond the first year. The conclusions will then necessarily be tentative.

The original concept was concerned with a battery with an energy density of up to 125 Wh/lb. It was intended to explore use of this battery to provide 500 "average driving" cycles. An average driving cycle was taken to provide a 20% depth of discharge for a 100 kWh battery. To reach the desired energy density, it was originally planned to use a V_6O_{13} positive electrode. During the course of the program, it became apparent that V_6O_{13} could not provide the required energy density. Therefore the last part of the program, involving construction and test of 20 Ah cells, was carried out with a MoS_3 positive electrode. Preliminary data had shown that MoS_3 could in principle approach the required performance. In practice it has turned out that MoS_3 needs further development and it may be unstable under cell-operational conditions.

The outline of the program was as follows:

Phase I. Conceptual Battery Design and Exploratory Experiments

Task I.1. Modeling

Model Li - solid cathode cells and batteries to optimize energy density. Basically, we first compared parallel plate stacks with bipolar cell arrays. The purposes were to identify the most weight sensitive components and to point the direction for design of the breadboard battery module to demonstrate the concepts (Phase II).

Task I.2. Critical Path Experimentation

The purpose was to find solutions to problems previously identified. Specific projects in hand were:

(a) Separators. A number of separators were evaluated for compatibility and efficacy in Li/V_6O_{13} cells.

(b) Overcharge mechanism. In particular for the bipolar plate array, we would need a chemical mechanism within each cell to accommodate overcharging. We looked at a number of promising redox couples such as I^-/I_2.

(c) Conductive polymers. It was thought that a bipolar plate array would be advantageous. A number of conductive polymers, notably carbon-filled polyolefins, were evaluated for use in a "bag-cell" bipolar array.

Phase II. Construction and Testing of Breadboard Battery Module

As the result of the work in Phase I, we designed and built breadboard cells to demonstrate the technology. The purposes of the demonstrations were:

(a) Energy Density: To show either >125 Wh/lb or the key problems limiting the energy density. These limitations can be divided into two (overlapping) classes: intrinsic limitations and engineering limitations. Intrinsic limitations could arise, for example, from inadequate electrode utilization, from the need to use excessive amounts of fillers and expanders to attain the desired rate, and from inadequate conductivity etc. etc. Engineering limitations could arise from inability in the time and budget frame of the program to select optimal component materials, structures and configurations. These inadequacies were factored out of the observed performance, and areas of most promise for weight/volume reduction readily identified. When we consider the optimization of electrode structure, as we must, the "intrinsic" and "engineering" aspects very much overlap.

(b) Cycle Life: To demonstrate 500 average driving cycles, or as many as possible, in view of the limited budget and time frame of the program. Every effort was made to identify life-limiting factors and project the ultimate cycle life.

2.0 PHASE I: CONCEPTUAL BATTERY DESIGN AND EXPLORATORY EXPERIMENTS

2.1 Task I. 1. Conceptual Design of the Automobile Battery

This was a modeling task for the critical examination of various automobile battery configurations. We were primarily concerned to compare a series cell arrangement employing bipolar electrodes and a parallel plate configuration.

Detailed diagrams of cell component configuration are presented in Figures 1 and 2. In the series arrangement individual cells are connected electrically across a conductive polymer between the cathode of one cell and the anode of the next. Current is conducted perpendicularly to the face of each electrode, insuring a relatively uniform current density and with very little weight added for bus-bars etc. Some 75 cells are connected in series in a battery unit having a total voltage between end collector plates of approximately 200V. Such units would then be connected in parallel, resulting in a battery assembly with increased current capacity at the same total voltage. In the case of a parallel plate configuration, individual plates are connected in parallel giving a unit cell of comparable size with voltage of approximately 2.5V. These units would be connected in series to achieve a battery assembly with the desired energy content.

A series-stack battery will necessarily be shaped somewhat like a book. The thinnest dimension, perpendicular to the electrode plates, will only be a few inches thick. For example, at 74 volts/inch, a 200 volt battery will only be ~3 inches thick. Higher voltages (and thicknesses) could be achieved, but are probably undesirable on safety grounds. As for the other two dimensions, they will probably be roughly equal, and on the order of a foot: In order to minimize the weight of the battery case, these two dimensions should be as large as manufacturability will permit. However, given the space available in an automobile, it is probably unrealistic for any dimension to exceed ~2 feet. Thus, the overall dimensions will likely be of the order of 12" x 12" x 3". This type of shape may also be required on thermal grounds: One relatively thin dimension is needed for effective heat dissipation.

In a parallel-plate battery, it is conceivable that a more nearly cubic geometry could be used, which would improve the energy density. However, thermal considerations may again require one of the dimensions to be relatively thin.

Combining these general considerations with energy and weight equations and energy loss equations, mathematical expressions for the energy density and volumetric energy density were derived in function of 40 cell

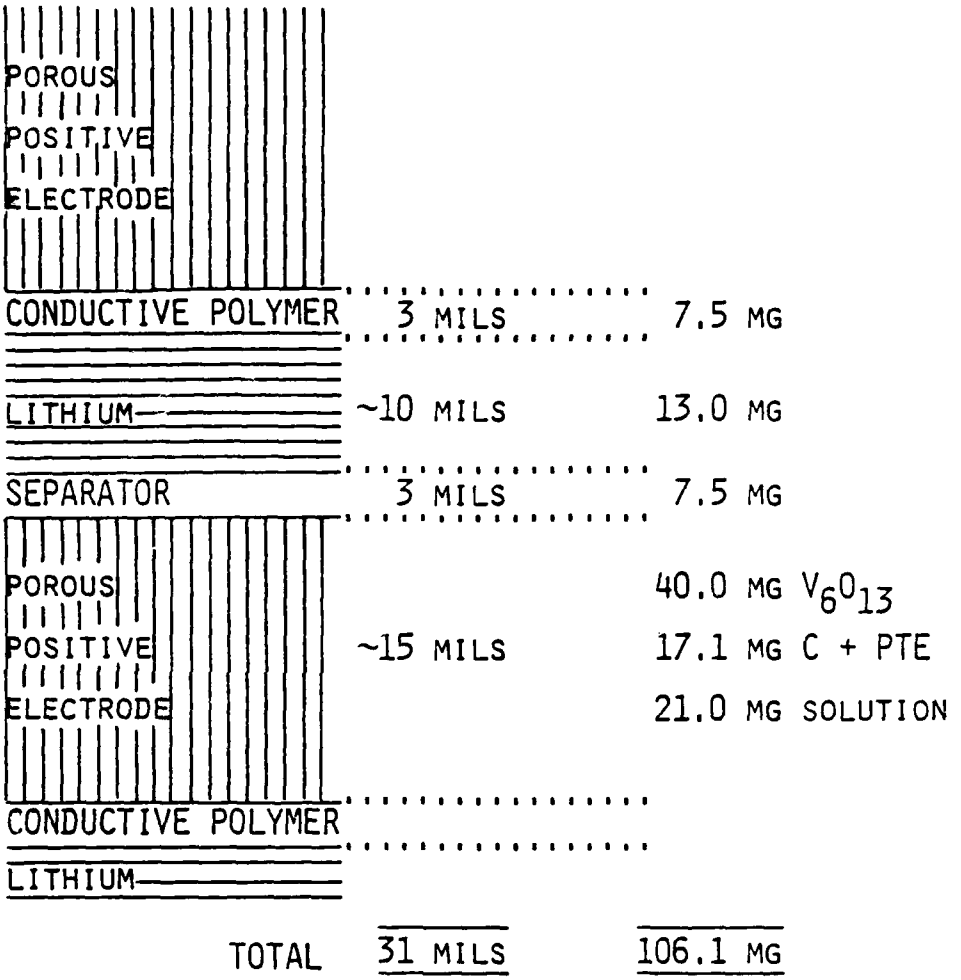

Fig. 1. Plastic bipolar plate cell.

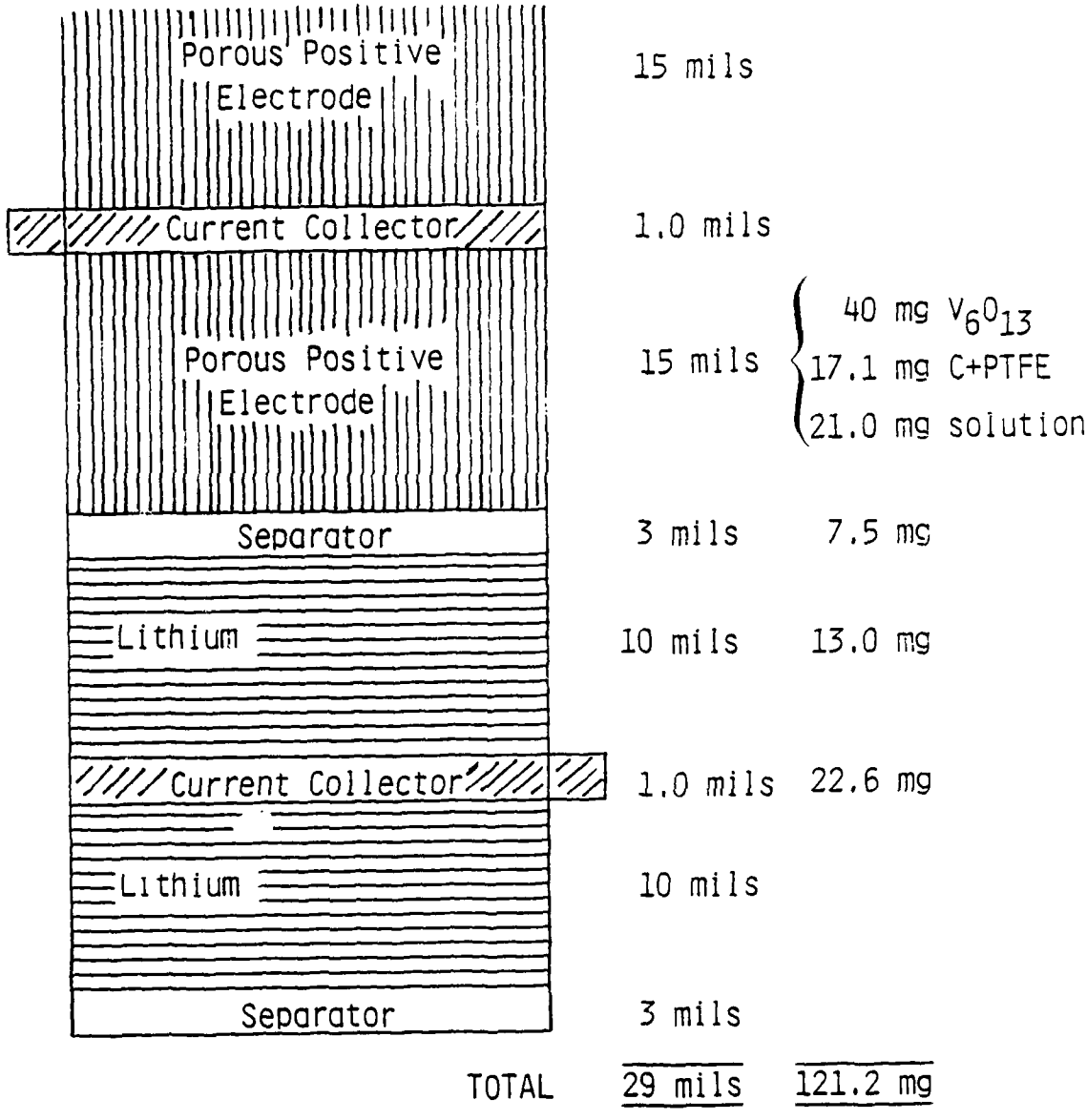

Fig. 2. Parallel plate cell configuration.

variables and coded for computer analysis. The variables and their default values are given in Table 1. Unless different values are specified, the default values are incorporated into the computer calculations. Energy density calculations were then done for materials presently in use and for other materials tested during the program.

These energy density calculations show no fundamental difference between parallel plate and series configurations. As suspected, the two most important parameters for cell energy density proved to be effective cathode energy density,

$$E_C = \frac{n \cdot 26.8 \cdot V \cdot f}{W}$$

where n = equivalent of charge/equivalent of mass; 26.8 = Ah/equivalent; V = average discharge voltage of Li cathode cell, f = fraction of active material in the cathode; W = equivalent weight of cathode and Li cycling efficiency. The influence of each of these parameters on total cell energy density is shown in Figures 3 and 4. Other factors including current collector thickness proved to have a lesser but nonetheless important effect. Current collectors 0.001" thick in use now in the parallel plate configuration lower the total cell energy density by about 11% from that given by a cell containing optimal current collectors.

Considering all these factors, the model shows that energy densities of over 100 Wh/lb are possible in parallel plate cells with MoS_3 as cathode material ($2.5e^-/MoS_3$), 0.001 inch Ni current collectors, which are presently in use, and 97.5% Li cycling efficiency (commonly obtained in actual laboratory cells). Achievement of the energy density goal of 125 Wh/lb may be possible at low discharge rates ($3.0e^-/MoS_3$). For a battery consisting of bipolar modules, an energy density of 115 Wh/lb is possible for high rate cycles ($2.5e^-/MoS_3$) and 135 Wh/lb is possible for low rate cycles.

A review of the modeling results shows that: (1) the most critical factor in attaining the energy density goal is the use of high energy density cathode material. The substitution of MoS_3 for TiS_2, which is the cathode we routinely use to exemplify rechargeable Li technology, increases battery energy density by 37% for $2.5e^-/MoS_3$ and by 65% for $3.0e^-/MoS_3$ when all other factors remain constant. (2) Li cycling efficiency is second in importance for battery energy density. An increase in cycling efficiency from 95% to 97.5% allows for a reduction in package size which translates into a decrease in container and excess electrolyte weight; if all other factors remain constant, this could result in a 30% increase in battery energy density. (3) To maximize energy density and attain the ultimate program goal, attention must be paid to engineering detail to minimize weight penalties from such cell components as current collectors. A diagram of such a battery is presented in Figure 5. In this bipolar configuration, a single current collector/substrate serves one

TABLE 1

PARAMETERS FOR ENERGY DENSITY CALCULATIONS

Cathode	Thickness	3.8×10^{-2} cm (15 mils)
	Porosity	60%
	Density	3.75 $g \cdot cm^{-3}$
	Weight fraction of active material	0.417
	Atomic weight of active material	50.942
	Electrons/gram-atom active material	0.8
	Resistivity	1000 ohm·cm
	Thermal conductivity	0.001 $W \cdot cm^{-1}\ {}^{o}C^{-1}$
Electrolyte	Density	0.92 $g \cdot cm^{-3}$
	Resistivity	250 ohm·cm
	Thermal conductivity	0.001 $W \cdot cm^{-1}\ {}^{o}C^{-1}$
Separator	Thickness	7.6×10^{-3} cm (3 mils)
	Porosity	60%
	Density	1.0 $g \cdot cm^{-3}$
	Resistivity	1000 ohm·cm
	Thermal conductivity	0.001 $W \cdot cm^{-1}\ {}^{o}C^{-1}$
Lithium	Thickness	2.92×10^{-2} cm (11.5 mils)
	Current efficiency	95%
	Cycle life	500 at 20% DOD
	Density	0.534 $g \cdot cm^{-3}$
	Resistivity	8.6×10^{-6} ohm·cm
	Thermal conductivity	0.75 $W \cdot cm^{-1}\ {}^{o}C^{-1}$
Conductive Polymer	Thickness	7.6×10^{-3} cm (3 mils)
	Density	1.0 $g \cdot cm^{-3}$
	Resistivity	1000 ohm·cm
	Thermal conductivity	0.001 $W \cdot cm^{-1}\ {}^{o}C^{-1}$
Current Collector	Thickness	3.4×10^{-4} cm (0.13 mils)
	Density	8.9 $g \cdot cm^{-3}$
	Resistivity	9.5×10^{-6} ohm·cm
	Thermal conductivity	0.6 $W \cdot cm^{-1}\ {}^{o}C^{-1}$
	Current plates per cell	2
Cell/Battery	Average voltage	2.4V
	Voltage of series package	200V
	Discharge time	Six hours
	Cell entropy	-20 $J \cdot mol^{-1}\ {}^{o}C^{-1}$
	Thickness of battery case	0.3 cm
	Density of battery case	1.0 $g \cdot cm^{-3}$
	Battery length	30 cm
	Battery height	30 cm
	Overall battery thickness (parallel plate battery)	10.0 cm

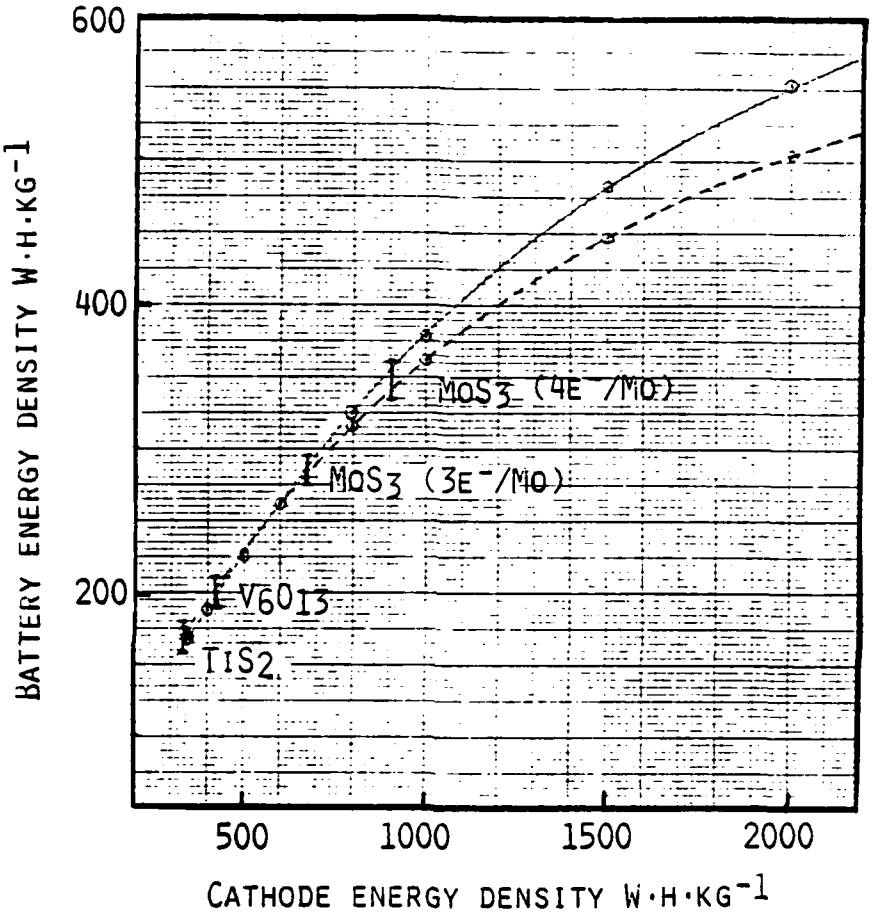

Fig. 3. Battery energy density as a function of cathode energy density.

—— Series

---- Parallel

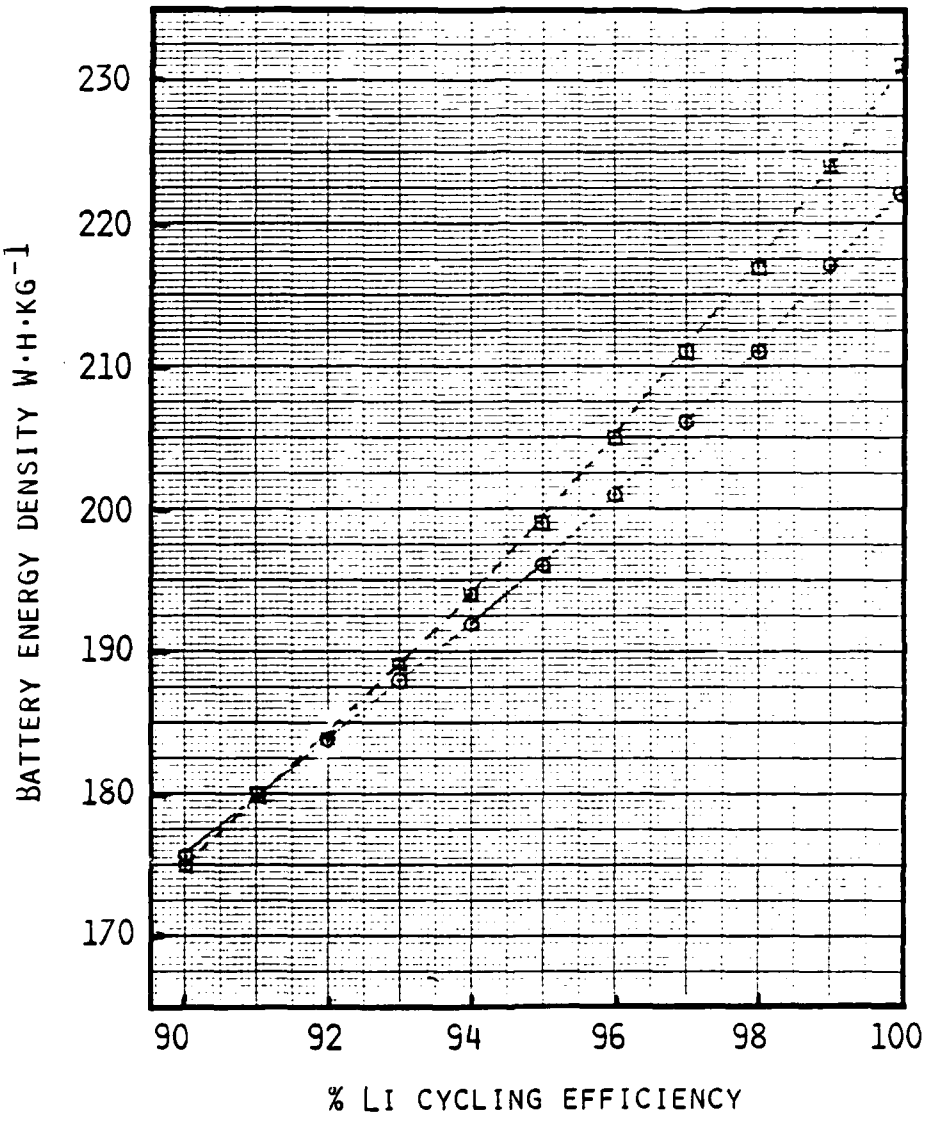

Fig. 4. Energy density as a function of Li cycling efficiency.

—— Stacked series arrangement

---- Parallel plate arrangement

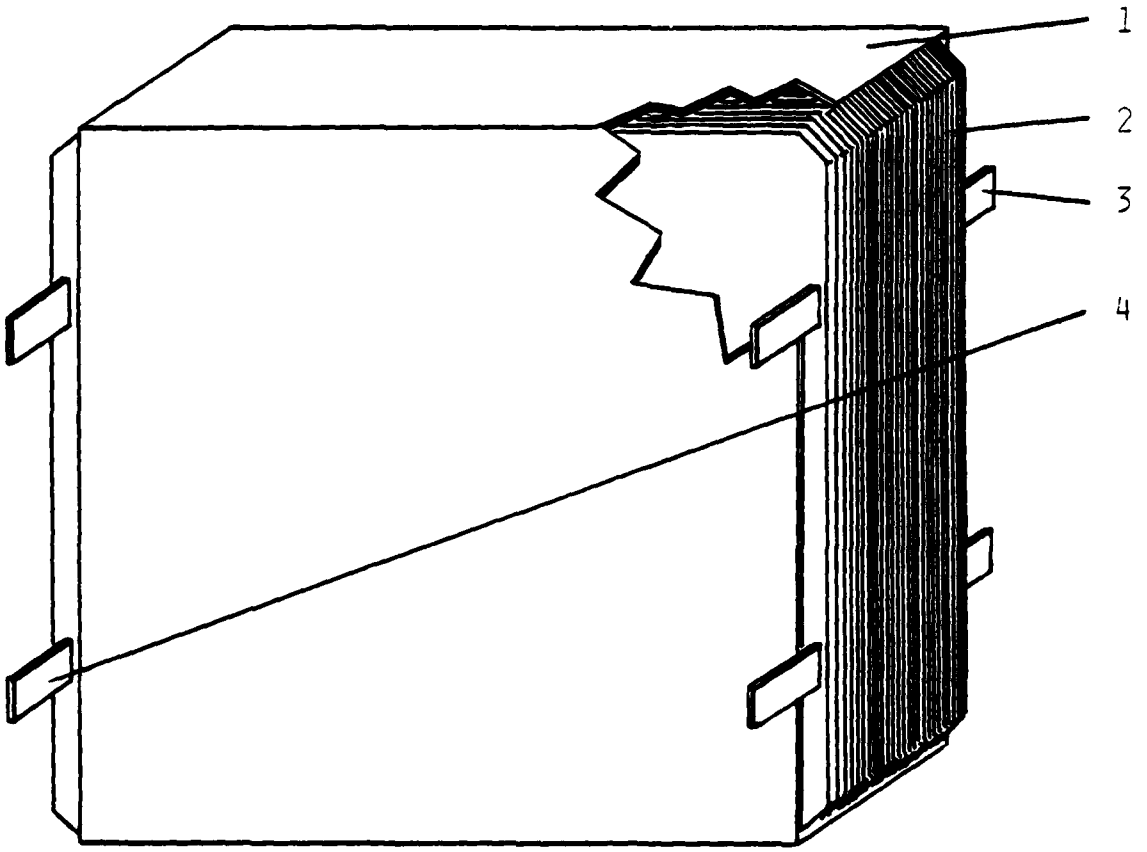

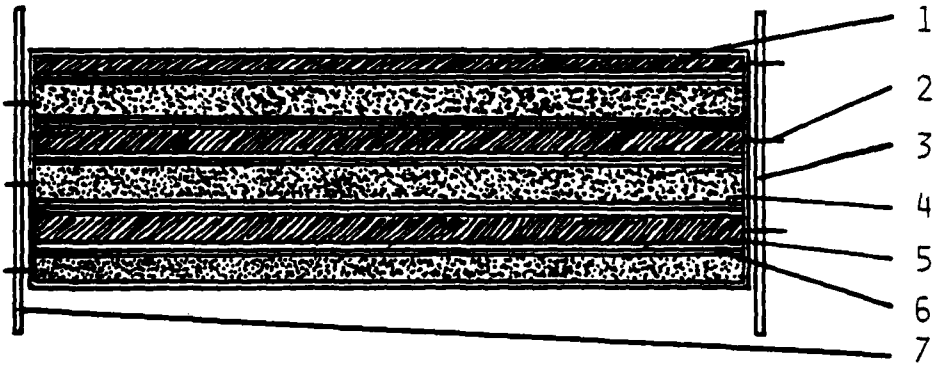

1. BATTERY CASE
2. CURRENT COLLECTOR
3. BUSBAR CURRENT COLLECTOR (-)
4. BUSBAR CURRENT COLLECTOR (+)
5. CATHODE
6. LI ANODE
7. SEPARATOR

Fig. 5. Parallel plate Li battery module.

anode and one cathode of adjacent cells. This substrate would be electronically conductive but impervious to ionic species. For such a battery configuration an energy density of 135 Wh/lb could theoretically be attained with MoS_3 cathode material.

2.2 Task I.2. Critical Path Experimentation

The critical path investigations were aimed at providing solutions to specific problems related to high energy density Li rechargeable batteries. The three major points of interest were: (1) choice of separator, (2) possible use of conductive polymers for bipolar electrodes and (3) to find an overcharge mechanism. Each of these phases of experimentation is discussed in turn.

2.3 Choice of Separator

Cell separators are necessary to avoid electronic shorting between the anode and cathode. The most important properties desired in separators are: (1) light weight for high energy density batteries, (2) flexibility and mechanical strength, (3) low ohmic resistance, (4) compatibility with the Li/2MeTHF-$LiAsF_6$/V_6O_{13} system with regard to solubility and chemical stability, (5) high lithium ion conductivity, (6) low electronic conductivity and (7) avoidance of lithium dendrite formation and subsequent shorting. Celgard microporous polypropylene membranes have been used successfully as separators in EIC lithium secondary cells but significant improvements in ohmic resistance and retention of Li dendrites were desired. A number of commercial and experimental separator samples were obtained and screened. The following separator materials from RAI were tested:

1. R1010, a sulfonated styrene graft on a one mil poly (tetrafluoroethylene) film (TFE).

2. R4010, a sulfonated styrene graft on a two mil TFE film.

3. R5010, a sulfonated styrene graft on a polyethylene membrane.

4. Polypropylene felt/SO_3H, a sulfonated styrene graft on a woven polypropylene membrane.

5. SP 126/SO_3H, a sulfonated styrene graft on a polypropylene mat.

6. 1128-71-1 and

7. 1131-21-1 porous experimental membranes containing sulfonic acid groups.

Other separator materials were obtained from Kimberly Clark and tested:

8. S49102, densified polypropylene.

9. S49680, barrier polypropylene.

10. S49696, polypropylene absorber.

11. S49796, cellulosic barrier, absorber.

Tests performed on these separators included:

(a) Continuous soxhlet extraction during 24 hours with pure 2Me-THF to evaluate membrane stability in the solvent. Each separator was evaluated for weight, dimension and texture changes; the solvent was analyzed by UV-IR spectrophotometry.

(b) Separator samples were stored in 1M $LiAsF_6$ in 2Me-THF while in contact with lithium metal and V_6O_{13} - graphite pressed electrodes for 10 days at 70°C. The separators, solvent and electrodes were evaluated for compatibility.

(c) Measurements were made of resistance through separator samples using a high frequency (10 kHz) constant current AC pulse and an oscilloscope to monitor the voltage drop across the experimental cell. This cell was constructed of two 2 cm^2 Li electrodes separated by one thickness of separator and close-packed with polypropylene spacers. The cell was then flooded with electrolyte and the measurements made.

(d) SEM micrographs of each of these separator materials were made and examined for porosity and microstructure.

2.4 Results of Separator Experiments

Results from the separator tests are presented in Table 2. No separator candidates more attractive than Celgard 2400 were found. Elimination from further consideration was possible for separators SP126, PP felt, Typar, S49680, S49696 and S49796 because of basic chemical incompatibility with the secondary Li cell environment; for separators R1010, R4010, R5010 and Tyvec because of low Li^+ conductivity in the electrolyte. Separator S49102, although chemically compatible, does not show any advantage over Celgard 2400 and, in fact, is thicker and has much larger pores which would facilitate dendrite penetration.

TABLE 2

RESULTS OF SEPARATOR TESTS

Separator	Dry Thickness (mils)	Results of Extraction Experiment	Results of Storage Test	Resistance $\Omega \cdot cm^2$	Porosity (SEM)
SP126 (RAI)	16.0	No significant change	Physical degradation		
PP Felt (RAI)	2.0	No significant change	Reaction with Li apparent		
R1010 (RAI)	2.0	No significant change	No significant change	>1000	Pores smaller than 1 μm
R4010 (RAI)	3.0	No significant change	No significant change	> 800	
R5010 (RAI)	7.5	No significant change	No significant change	>1000	Pores smaller than 1 μm
Tyvec (RAI)	16.5	No significant change	No significant change	260	≥10 μm
Typar (RAI)	10.0	16% weight loss, physical degradation			
S49102 (KC)	3.0	No significant change	No significant change	19	~50 μm
S49680 (KC)	6.0	17% weight loss	Slight discoloration		
S49696 (KC)	7.0	14% weight loss	No significant change	21	~20 μm
S49796 (KC)	11.5	31% weight loss	Reaction with Li apparent		
Celgard 2400	1.0	No significant change	No significant change	21	Regular pores 0.02 x 0.2 μm

2.5 Conductive Polymers for Bipolar Electrodes

Significant improvements in energy density can be expected in batteries containing conductive polymers between cells. Plastic polymers are light in weight and in a bipolar electrode arrangement they eliminate the need for heavy bipolar metal grids and collectors. In this battery arrangement the current can be collected at the extreme poles of the alternating electrode stack. As the passage of current is perpendicular to the plane of the conductive polymer/bipolar electrode, the current density across the relatively large surface should be low and polymers with only fair conductivity may be of interest. These polymers should have good mechanical strength and flexibility even when thin films are used. They must have chemical stability in the system and they must conduct electronically and not ionically.

A preliminary test of the solvent compatibility of seven conducting and semiconducting polymers was done simply by immersing samples of each in freshly distilled 2Me-THF and allowing them to sit at room temperature over three days. The polymers tested include:

1. Velostat (3M)
2. Dev 9436 (Carbon filled thermoplastic, Pervel Ind.)
3. Dev 9437 (Carbon filled thermoplastic, Pervel Ind.)
4. 2 mil (Carbon filled thermoplastic, Pervel Ind.)
5. 3 mil (Carbon filled thermoplastic, Pervel Ind.)
6. Antistatic film (Semiconducting vinyl copolymer, Pervel, Ind.)
7. Polyphenylene sulfide (PPS, Phillips Petroleum).

The 2 mil carbon-filled plastic from Pervel Industries is presently used in Polaroid camera alkaline batteries. Among these seven polymeric films only the Velostat and PPS showed any stability in 2Me-THF. All five of the Pervel plastics disintegrated or dissolved in the solvent.

The Velostat film was shown to be permeable to Li^+ ions making it unsuitable as a substrate for bipolar electrodes.

The PPS film was the only plastic tested which was physically compatible with the electrolyte solution. However, its high resistivity indicated that doping was not accomplished either electrochemically or by reacting with either n-butyllithium or I_2 over the period of a week. If a

suitable doping procedure is discovered, this may become a usable conductive polymer in the future. Another candidate for the conductive polymer was polyacetylene. However, because of its open pore structure it was unsuitable for our purposes. To date we have not been able to identify a conductive polymer which would be suitable as a bipolar electrode substrate in rechargeable ambient temperature Li battery.

2.6 Overcharge Mechanism

In a multiple-cell battery employing bipolar electrodes, a mechanism is necessary for insuring nearly equal charge and/or discharge in each of the separate cells to avoid electrolysis of the solvent after repeated cycles. One method of avoiding this problem is to employ an overcharge mechanism which will shunt current through a fully charged cell above a certain potential. This would allow for overcharging the battery as a whole. Chemical redox pairs with formal potentials above the cathode potential and below the potential corresponding to solvent electrolysis should be suitable for this if (1) both oxidized and reduced species are soluble in the solvent, (2) the reduced species is chemically compatible with all cell components, (3) the oxidized species is compatible with all cell components except the anode and (4) both oxidized and reduced species are able to diffuse through the separator. I^-/I_2, ferrocene/ferricinium, chloranil/chloranilate and fluoranil/fluoranilate couples were investigated. Each of these couples were shown to have a redox potential in the correct range by cyclic voltammetry.

Chloranil/chloranilate and fluoranil/fluoranilate proved unacceptable as overcharge redox couples because of insolubility and irreversible film deposition on Li electrodes. The I^-/I_2 couple was shown to be capable of carrying the desired current density of 1 mA/cm^{-2} but seems to have caused the failure of cycled cells containing it, possibly by means of film formation on the Li electrode or reaction with the solvent/electrolyte. The ferrocene/ferricinium couple was shown to be incapable of carrying current densities of 1 mA/cm^{-2} but may prove interesting for low rate charge. More work on these two redox couples is needed to evaluate their long term cycling effects in complete Li/cathode cells. Although an acceptable chemical shuttle for overcharging a secondary Li cell was not found, we found no fundamental flaw in the concept of chemical overcharge.

3.0 PHASE II: CONSTRUCTION AND TESTING OF BREADBOARD DEMONSTRATION MODULES

3.1 Design of Demonstration Module

Calculations for the design of the demonstration module were based on a MoS_3 cathode which has been shown by K. M. Abraham[1] to be able to deliver a current density in excess of 1.5 $mA \cdot cm^{-2}$ with a 30% carbon loading in the cathode to guarantee good conductivity.

Several can sizes and shapes were considered for the design of the battery. A can with the largest face open (that is the face parallel to the electrode faces) was chosen for the following reasons: (1) placement of the battery package in the can is facilitated since compression of the package is accomplished after rather than during placement in the can; (2) compression of the package is easily controlled by using more or fewer electrodes; (3) the battery capacity can easily be changed without changing electrode size by cutting the can to the proper depth; (4) welding the cathode or anode leads together can be achieved after placement of the battery package into the can.

A commercially available can with outer dimensions 10 cm x 11.75 cm x 4.125 cm (Hudson Tool and Die Co., Inc., Newark, NJ, can #7640) was chosen. Allowing for 36 mil can walls (0.091 cm) and 0.2 cm excess space on all edges, 1.5 cm on the end for leads, and 0.025 cm (10 mils) for a protective Teflon sheet on the top face nearest to the cover weld; the battery package dimensions are 9.51 cm x 10.16 cm x 3.37 cm. The can depth, of course, could be cut to smaller dimensions. A 20 Ah battery discharged at a 6 h rate must be able to deliver 3.33A. At 1.5 $mA \cdot cm^{-2}$, this corresponds to a cathode area of 2222 cm^2 or 23 electrode faces with the dimensions given above (96.62 cm^2). Thus, we have a total of 11 two-faced cathodes. Assuming we obtained $2.5e^-/MoS_3$ for a mixture of MoS_3 (70%) and C + PTFE (30%) with a 50% porosity, we need 63.0 cm^3 of cathode material. This corresponds to 0.029 cm (11.5 mils) of this material pressed onto each cathode face for a capacity of 9.41 mAh/cm^2.

The Li anodes must have a 5-fold excess capacity for 100 full discharges at 95% plating efficiency. Thus they had at least 10 mils Li pressed onto each active face.

The total battery package including anodes, cathodes, current collectors, separators and a 10 mil protective PTFE sheet were approximately 1.49 cm thick.

---

[1] K. M. Abraham and S. B. Brummer in "Lithium Batteries", J. P. Gabano Ed., Academic Press, London, book in print.

Because of the expense involved in ordering custom tooling and manufacture of optimized cans, the commercially available product with specifications closest to our needs was chosen. It is important to note; however, that by using cans of 0.036" thick walls, the overall sacrifice in cell energy density is quite significant. A diagram of the cell is given in Figure 6 and parameters in Table 3.

3.2 Construction of the Modules

3.2.1 Preparation of the Cathode Material

The cathode material was synthesized via a two step procedure:

$$(NH_4)_2MoO_4 + 4H_2S \xrightarrow{NH_4OH} (NH_4)_2MoS_4 + 4H_2O, \quad (1)$$

$$(NH_4)_2MoS_4 \xrightarrow{\Delta} MoS_3 + (NH_4)_2S. \quad (2)$$

Reagents: Ammonium paramolybdate from Alfa Inorganics, [$(NH_4)_2Mo_7O_{24} \cdot 4H_2O$, Stock #87346]; con·$NH_4OH$ reagent; tank of H_2S.

In a typical synthesis, 120 gms of the ammonium molbydate is dissolved in 600 ml of con·NH_4OH with stirring. H_2S is bubbled through the stirred solution for five hours. The solution initially turns red upon reaction with H_2S. Within one hour, yellow-white crystals, presumbly $(NH_4)_2MoO_{4-x}S_x$, precipitate. The crystals dissolve during the second hour of the reaction leaving a clear, deep red solution. By the third hour red crystals of $(NH_4)_2MoS_4$ begin to precipitate. The reaction should be complete in five hours.

The red crystals are vacuum filtered and washed with ~100 ml of NH_4OH. Excessive washing will dissolve the product. The product is then dried under mild heating in vacuum. The yield typically is >95%. The product is stable in air. However for extended storage it should be kept in an argon atmosphere.

A weighed amount of the $(NH_4)_2MoS_4$, contained in a graphite boat inside a glass tube, is heated in a tube furnace under a flowing argon atmosphere at 300°C for three hours. After the heating, the system is cooled to room temperature. The black MoS_3 product is transferred to the glove box with minimal exposure to air. The yield is 100%.

All batches of MoS_3 produced were chemically analyzed for composition and sample electrodes from each batch were tested. Batches 2, 5, 6, 7 and 8 with analyses from $MoS_{2.95}$ to $MoS_{3.12}$ gave also acceptable electrochemical performance. Characteristic cycle performance of a pressed cathode from MoS_3 Batch No. 7 with practical loading is shown in Figure 7.

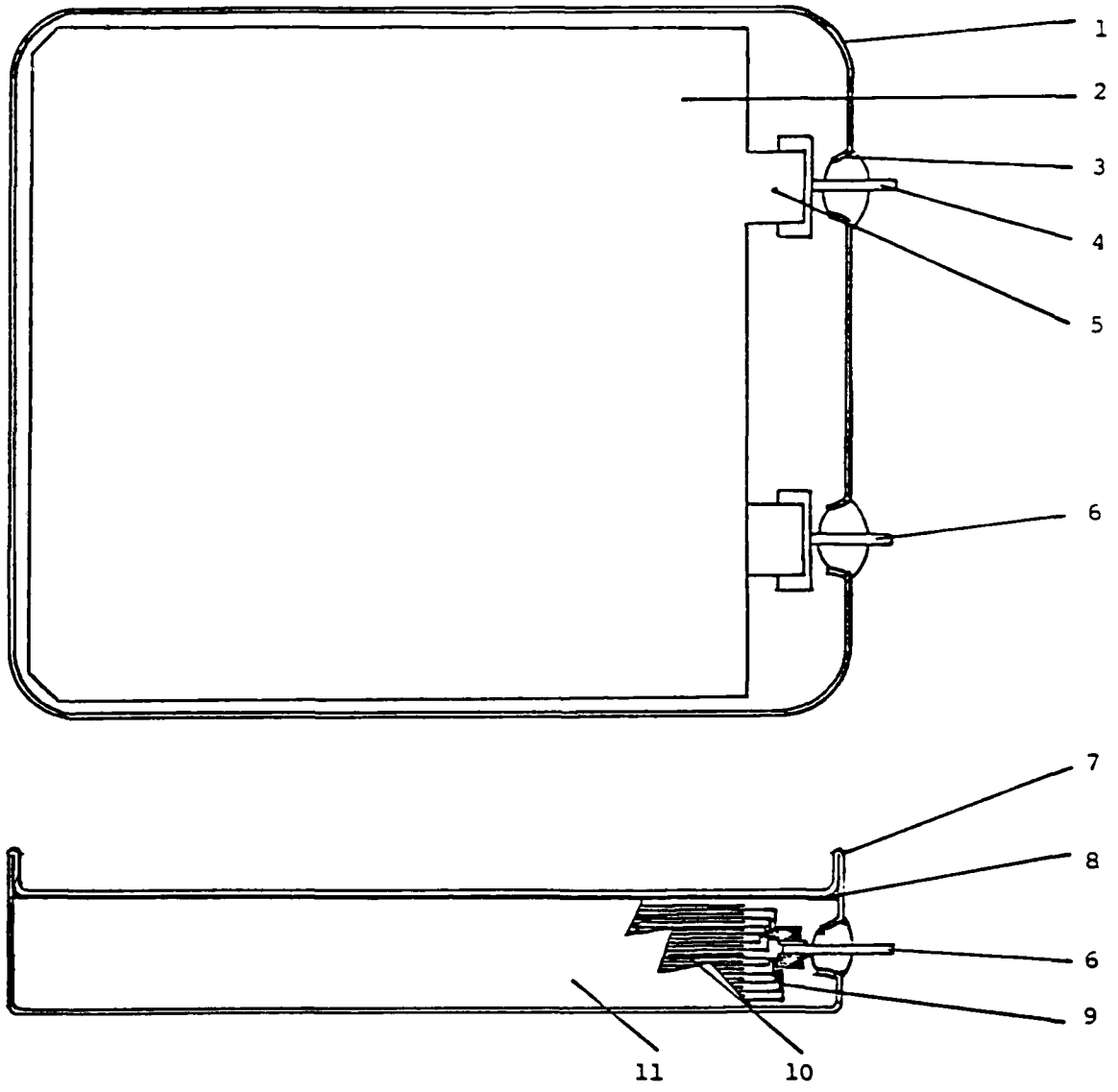

1. Hudson can #7640
2. Negative electrode
3. Glass to metal seal
4. Negative terminal
5. Lead to negative terminal
6. Positive terminal
7. Can-cover weld
8. PTFE sheet
9. Leads to positive terminal
10. Alternating electrodes with 2 layers Celgard 2400 between each pair
11. Celgard 2400

Fig. 6. Design for 20 Ah secondary Li battery.

TABLE 3

DESIGN PARAMETERS FOR $Li//MoS_3$ BATTERY

Hudson Can No. 7640
Outer dimensions 10.0 cm x 11.75 cm x 4.125 cm
Inner dimensions 9.91 cm x 11.66 cm x $\leq$3.40 cm

Capacity	20 Ah	25 Ah
Can depth	1.58 cm	2.54 cm
Electrode size	96.6 cm^2	96.6 cm^2
Number of cathodes	11	14
Number of anodes	12	15
Package thickness	1.49 cm	1.79 cm
Package weight	234 g	296 g
Projected package energy density	162 $Wh \cdot kg^{-1}$	176 $Wh \cdot kg^{-1}$
Projected package volumetric energy density	220 $Wh \cdot \ell^{-1}$	230 $Wh \cdot \ell^{-1}$
Can weight	245 g	270 g
Projected battery energy density	79 $Wh \cdot kg^{-1}$	85 $Wh \cdot kg^{-1}$
Projected battery volumetric energy density	193 $Wh \cdot \ell^{-1}$	215 $Wh \cdot \ell^{-1}$

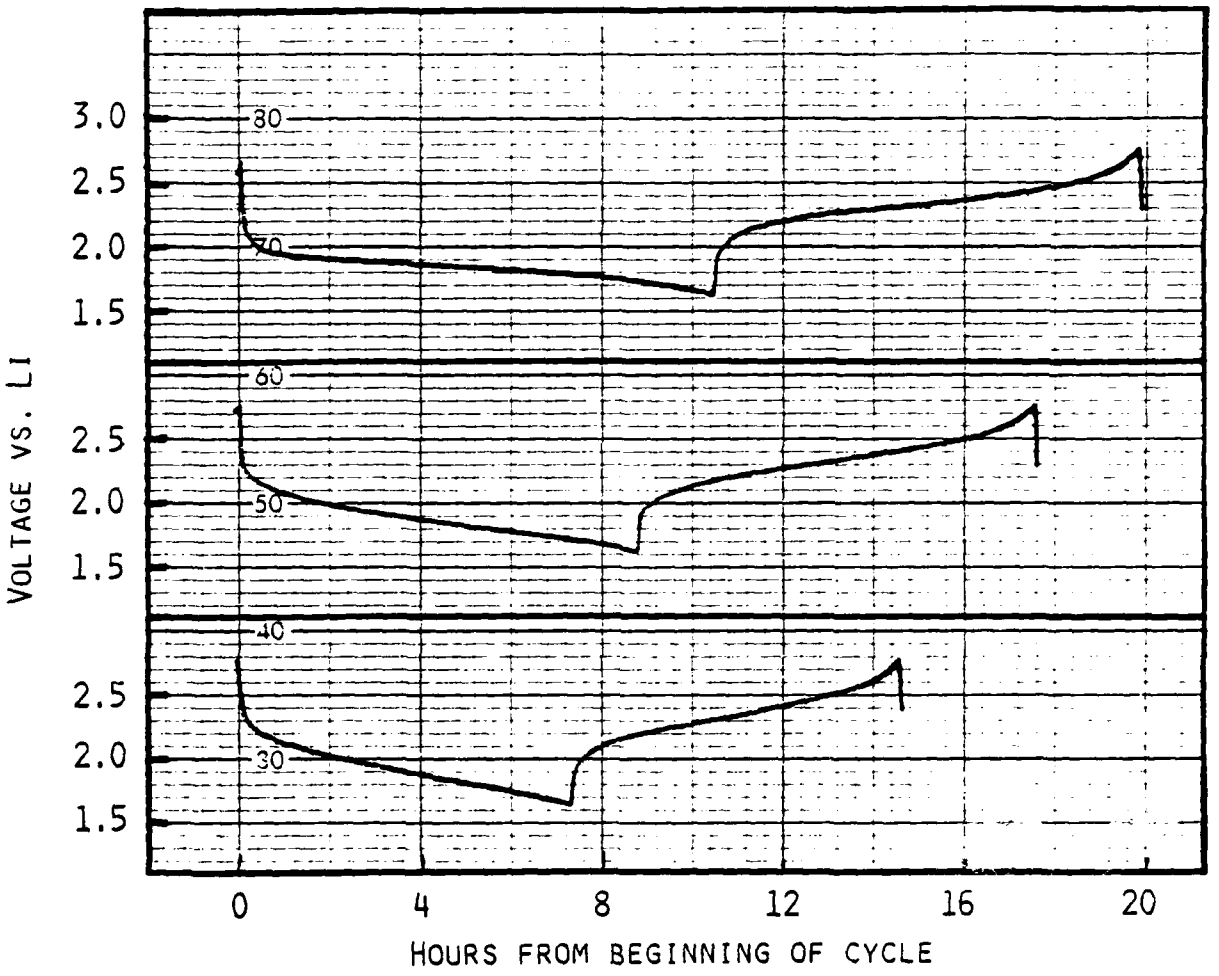

Fig. 7. Charge-discharge cycles of a MoS_3 electrode (65% MoS_3 Batch 7, 30% C, 5% PTFE) with design loading level at a current density of 1 mA/cm^2. Shown are cycles 1, 3 and 25.

3.2.2 Effect of Carbon on Rate and Cathode Utilization

These studies were carried out with low capacity cathodes, typically 2-3 mAh/cm^2 based on 1e$^-$/MoS_3.

Figure 8 shows the effect of carbon content on rate capability and cathode utilization. The data were obtained from three different cells. Each cathode was discharged at current densities of 0.5, 1, 2, 3, 4, 5 and 6 mA/cm^2. After each discharge the cathode was recharged to 3V at 0.5 mA/cm^2 to obtain the capacity at the next rate. The cathode containing 30 w/o carbon showed the best performance, yielding capacities between 2 and 3e$^-$/MoS_3 at current densities between 4 and 0.5 mA/cm^2.

3.2.3 Rechargeability of MoS_3

The material intrinsically has good rechargeability. However, the rechargeability is dependent on the amount of carbon in the cathode. Thus the cathode with 30 w/o carbon exhibited the highest retention of capacity with cycling. This is shown in Figure 9. Thus at a current density of 1 mA/cm^2, the capacities were 3e$^-$/MoS_3 at the third discharge, 2.7e$^-$/MoS_3 at the 20th discharge and 2e$^-$/MoS_3 at the 46th discharge. The capacity faded to 1.6e$^-$/MoS_3 by the 57th cycle. However, when the current was reduced to 0.5 mA/cm^2 at the 58th discharge, the cathode utilization increased to 2.65e$^-$/MoS_3.

3.2.4 Preparation of Cathodes

Various methods were investigated for the fabrication of uniform electrodes of sufficient mechanical strength for handling and cell assembly. The procedures of cathode preparation are further restricted by the fact that the electrodes must be free of contaminants which could interfere with the rechargeability of the Li electrode. Smaller test electrodes were generally prepared by pressing of powder mixtures in a suitable die. Scale-up of this process is made difficult by the poor flow characteristics of the Teflon containing powders. This causes uneven material distribution and poor adhesion after compaction. We pursued an alternative procedure involving the preparation of a paste which could be spread evenly onto a substrate. Decane was identified as an inert solvent for this purpose. Complications arose from the coagulation of graphite containing slurries and the poor adhesion in the absence of graphite. The mode of grinding and mixing of the MoS_3, C, TFE powders also substantially affects the consistency and workability of the pastes. As a result of this experimentation, we identified a procedure to prepare electrode structures of appropriate size with 10 mAh/cm^2 per side and a composition of 65% MoS_3, 30% C and 5% TFE. The process involves grinding-mixing of the powders, pasting a layer of controlled thickness onto both sides of a substrate and pressing.

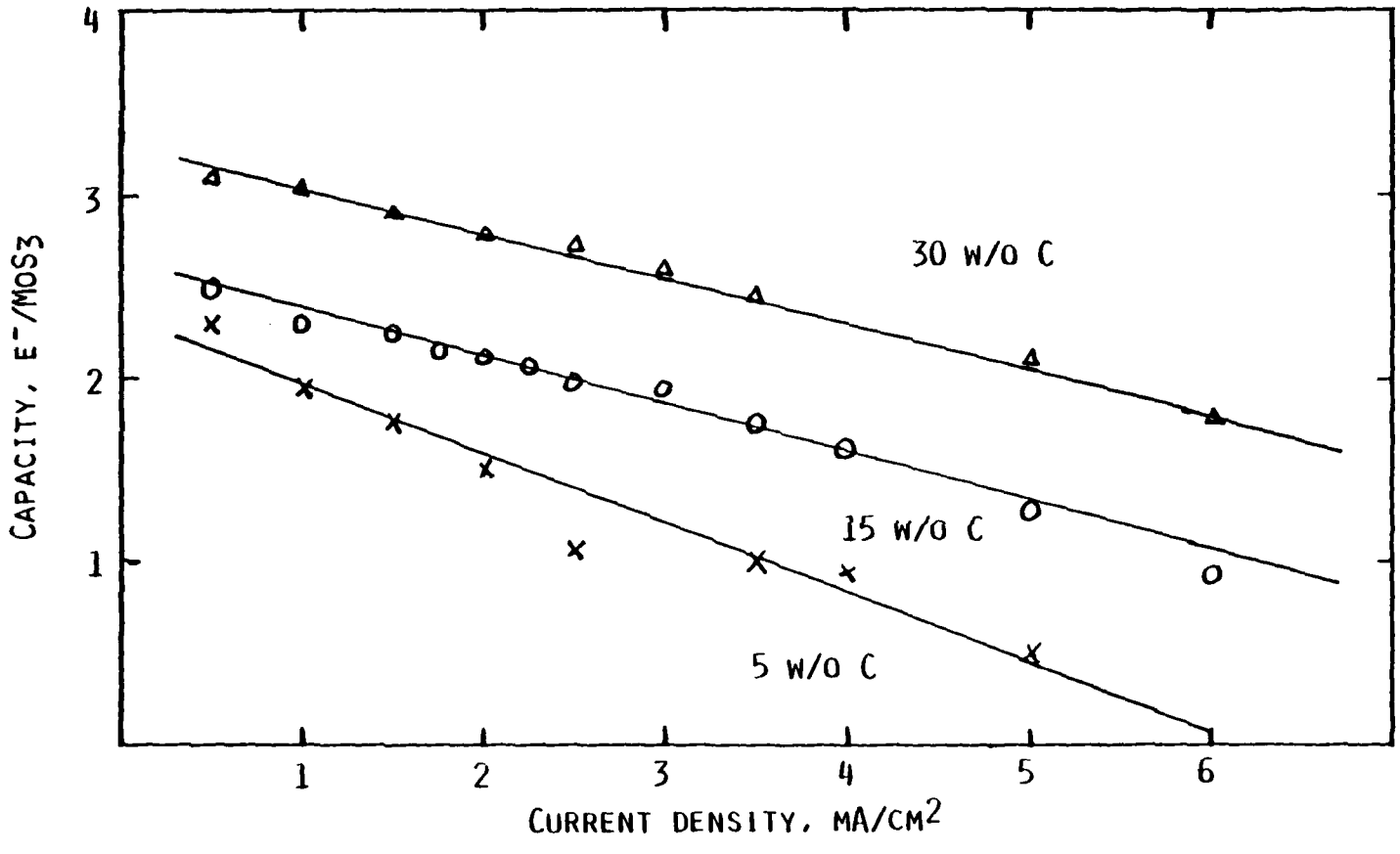

Fig. 8. Cathode utilization versus current density as a function of carbon in the cathode. The cell utilizes 2Me-THF/1.5M $LiAsF_6$.

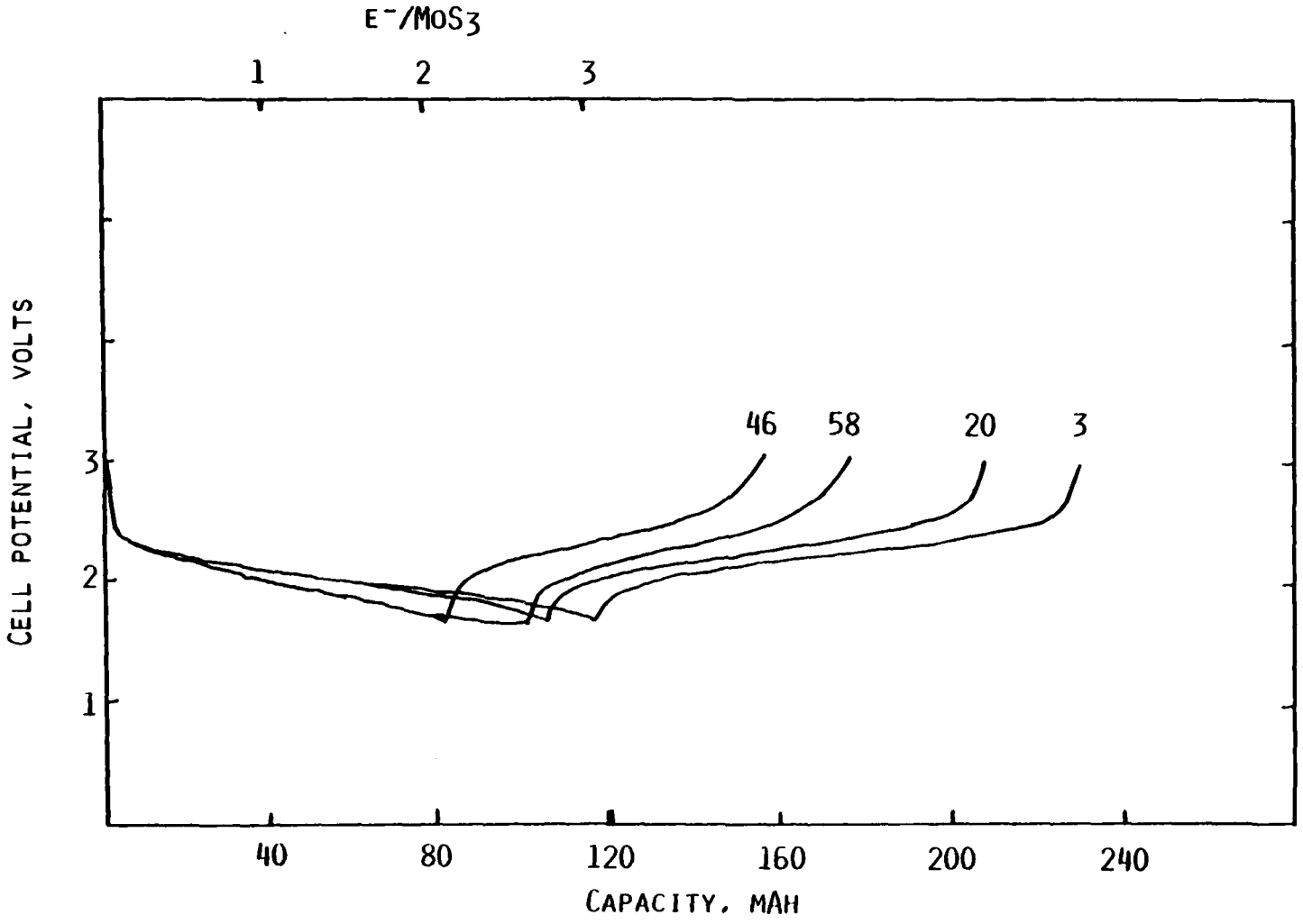

Fig. 9. Typical cycles of Li/MoS_3, 30 w/o, 2Me-THF/1.5M $LiAsF_6$ cell. Current = 20 mA (1.0 mA/cm^2) for cycles 3, 20 and 46; 10 mA (0.5 mA/cm^2 for cycle 58. Cycling limits 1.6 ⟷ 3 volts.

The positive electrode substrate consists of a 1 mil nickel foil which is pierced from both sides, resulting in holes of 14 mil diameter and burrs of ~7 mil. The substrate has solid borders to reduce the danger of damage of the separator which might result in dendrite shorting of the cell. The finished cathodes were 35-40 mils thick. In the described manner we obtained good electrode structures. However, their electrochemical performance was not optimized with respect to composition, active material loading or process variables.

3.2.5 Preparation of Anodes

The anodes were prepared by pressing 10 mil Li foil for Cell 1 and 15 mil Li foil for the other four cells onto each side of an expanded nickel screen. The tab consisted of two 5 mil thick, 0.2 in. wide Ni strips.

3.2.6 Preparation of Cell Cases

The stainless steel cases obtained from Hudson Tool and Die Company were sent out to be fitted with two glass to metal terminal feedthroughs. The terminal pins consist of hollow tubes to allow filling with electrolyte. A comb was manufactured and welded to the inside terminals to accept the individual electrode tabs. Despite rework, the can-cover fit was insufficient, especially in the corners, to allow hermetic cell closure by TIG welding. A tool was fabricated which allowed appropriate stretching of the covers.

3.2.7 Cell Assembly

Anodes and cathodes were heat sealed into bags of Celgard 2400 separators and alternatively stacked into the cell case. Cell 5 had an extra layer of Celgard 2400 Z-folded around the electrodes to afford extra protection against dendrite shorting. The latter contained a liner of a FEP membrane. The electrode tabs were joined to the bus bar comb by TIG welding. The completed electrode assembly was compressed, the cover secured by spot welds and subsequently hermetically sealed by a TIG weld.

3.2.8 Cell Activation

The completed cell was activated by vacuum filling with 91.5 cm^3 of 1.3M $LiAsF_6$ in 2Me-THF prepared by EIC established procedures. This amount of electrolyte covers the plates by approximately 0.5 cm. Subsequently the fill holes were hermetically sealed by TIG welding.

Photographs of some completed 20 Ah cells are presented in Figure 10.

Fig. 10. 20 Ah prismatic Li/MoS_3 cells.

3.3 Testing of the Modules

3.3.1 Test Plan

The primary objective was to determine and demonstrate cycle life and collect data to project the performance capability of the system. The following is a summary of the test plan followed for the five cells.

1. Inspect and weigh cell, measure open circuit voltage.

2. Three or four full discharge-charge cycles at 2A. Discharge to 1.6V, charge to 2.8V.

3. Continuous cycle test to capacity limit. Discharge to between 60 and 70% depth based on 2nd-4th discharges. Charge to 2.8V or discharge capacity + 10%, whichever comes first. Every 20 cycles perform a full discharge to 1.6V. Continuously record voltage vs. time.

4. Reduce current as necessary when capacity falls off.

5. Continue cycling to failure defined either by loss of capacity or short-circuting.

6. Evaluate effect of charge and discharge rates on capacity while maintaining constant the discharge and charge rates respectively.

All five cells were carried through Steps 1 and 2. One cell was reserved for Step 5 and the others continued through Steps 3-5.

3.3.2 Characterization of the Modules

Weights, capacities (based on $2.5e^-/MoS_3$) open circuit voltages and energy densities are presented in Table 4. These energy densities are based on 2.5 e^-/MoS_3, actually obtained at rates approaching C/40.

3.3.3 Cycle Testing of the Modules

All five cells were discharged to 100% DOD and charged for four cycles in order to evaluate cell capacities at C/10 rate. As cell 1 failed by dendritic short circuit on the third cycle, Cells 2, 3 and 5 were reserved for cycle life testing and only one, Cell 4, was reserved for rate studies.

Results of the cycle life demonstration are given in Table 5. After the initial deep discharge cycles, the cells were discharged to between 60 and 70% depth of discharge until failure. A typical 100% cycle is represented in Figure 11.

TABLE 4

Li/MoS_3 CELL PARAMETERS

Cell No.	Package & Electrolyte Weight (g)	Open Circuit Voltage (V)	Capacity Based on $2.5e^-/MoS_3$ (Ah)	Package Energy Density (Wh/kg)
1	304	3.28	24.2	151
2	320	3.15	25.1	149
3	345	3.32	25.0	138
4	331	3.40	24.9	143
5	328	3.30	24.7	143

TABLE 5

20 Ah Li/MoS_3 CELL CYCLE TEST

Cycle Number	Cell 2		Cell 3		Cell 5		
	C, Ah	MDV, V	C, Ah	MDV, V	C, Ah	MDV, V	Comments
1	20.3	1.86	18.1	1.90	18.2	1.90	
3	19.8	1.90	18.8	1.90	16.3	1.93	
5	12.0	2.05	12.0	1.98	12.0	2.00	
10	14.0	2.05	12.0	1.99	12.0	1.95	
15	14.0	2.04	12.0	1.93	12.0	1.93	
20	14.0	1.88	12.0	1.97	12.0	1.93	Cell 2 soft short
30			12.0	1.90	12.0	1.92	
35			8.6	1.83	11.5	1.90	Cell 3 soft short
45			12.0	1.90	7.7	1.91	Cell 3 recovered
50			9.8	1.85	6.0	1.92	Cell 3 soft short
52					18.7	1.97	I reduced, 0.25A

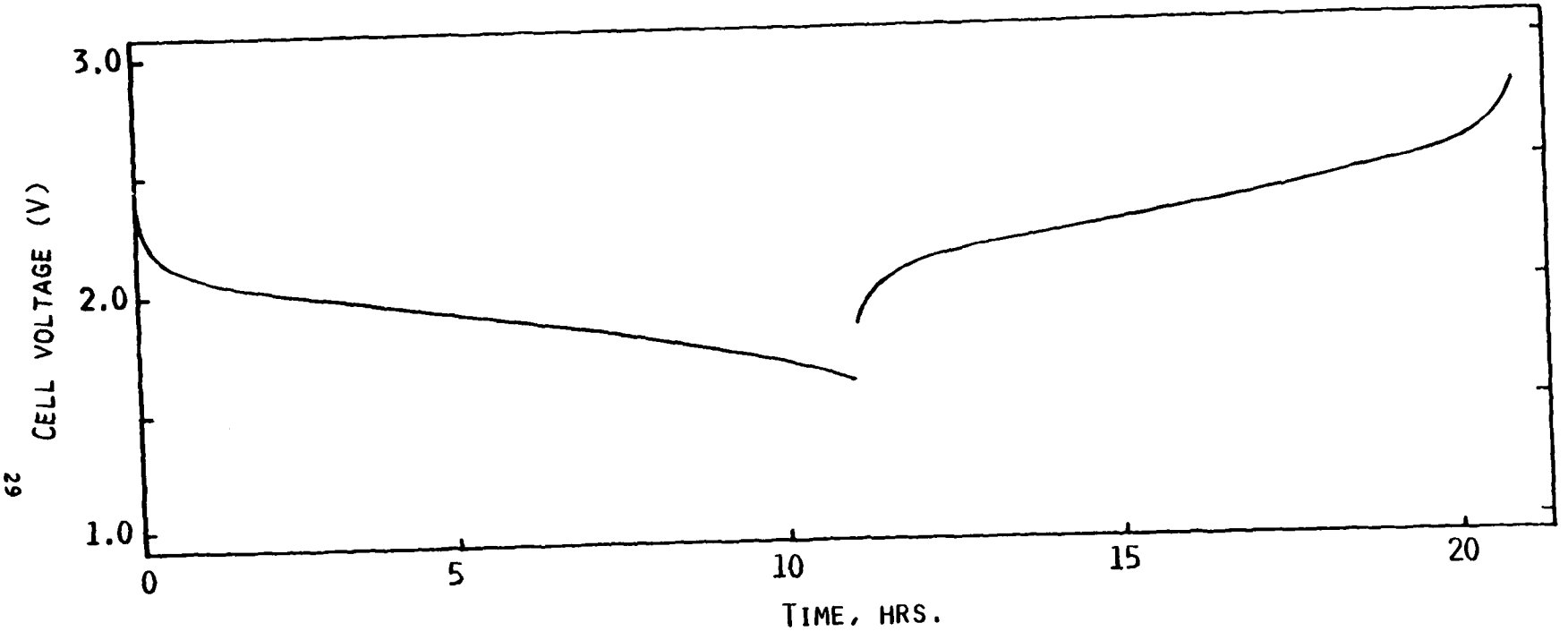

Fig. 11. Li/MoS_3 cell discharge-charge cycle at 2A.

Cell 2 developed dendritic shorting by the 20th cycle and was terminated when it was overdischarged to 0.2V. Cells 3 and 5, however, each completed more than 50 discharge/charge cycles before being terminated. After 35 cycles, Cell 3 developed a "soft short" or a short circuit by dendritic bridging which forms during charge (usually towards the end of the half-cycle) and disconnects during discharge. This cell recovered by the 42nd cycle and continued to cycle well until the recurrence of more stable dendrites, "hard shorts", forced the cell to lose capacity and overdischarge after 52 cycles. Cell 5 completed 50 cycles until loss of capacity became extreme. This cell was then cycled at a low rate (0.25A or 0.1 $mA \cdot cm^{-2}$) to determine whether the decline in capacity was due to a change in the cathode material or to an increase in cell resistance. The large capacity, 18.7 Ah (actually greater than that of the first cycle), indicates that the cathode material was still intact and functional. An increased cell resistance must therefore be responsible for the performance loss. This cell was removed from the cycling regime after completing 56 cycles.

Results from the rate study done with Cell 4 are shown in Figure 12. At the C/10 and C/20 rates this cell demonstrated little difference in discharge capacity, corresponding to approximately $2e^-/MoS_3$. At lower rates (C/40) the cell capacity reached 24.3 Ah, which corresponds to $2.44e^-/MoS_3$.

3.4 Tear Down Analyses

Several of the cycled cells were opened for analysis. This included physical measurements of the cathodes, anodes and cells as a whole; X-ray diffraction and elemental analyses of the cathodes and anodes; conductivity measurements of the electrolyte solution; microscopic examination of anodes, cathodes and separators; and cycling tests of refilled cells. Results of these analyses are given in the following paragraphs.

3.4.1 Physical Measurements

Measurements were performed on Cell 3 which had failed by shorting and overdischarge after 53 cycles. A figurative diagram of the cell and measurement positions is shown in Figure 13; the measurements before and after cycling are given in Table 6. A fill tube of this cell was opened and after removal of electrolyte solution, propylene carbonate was added to passivate the highly reactive Li deposits present. The cathodes from this cell were then removed and found to have expanded an average of about 30% from approximately 0.040" to 0.053" each. Some package expansion is also due to conversion of the solid Li anodes to a porous mud-like form.

3.4.2 Electrolyte Addition

The internal resistance of Cells 2-5 after cycling was 10Ω, 20Ω, 4Ω and 12Ω, respectively. All cells but Cell 5 had been overdischarged. Electrolyte solution was removed from Cell 3 and its specific resistivity

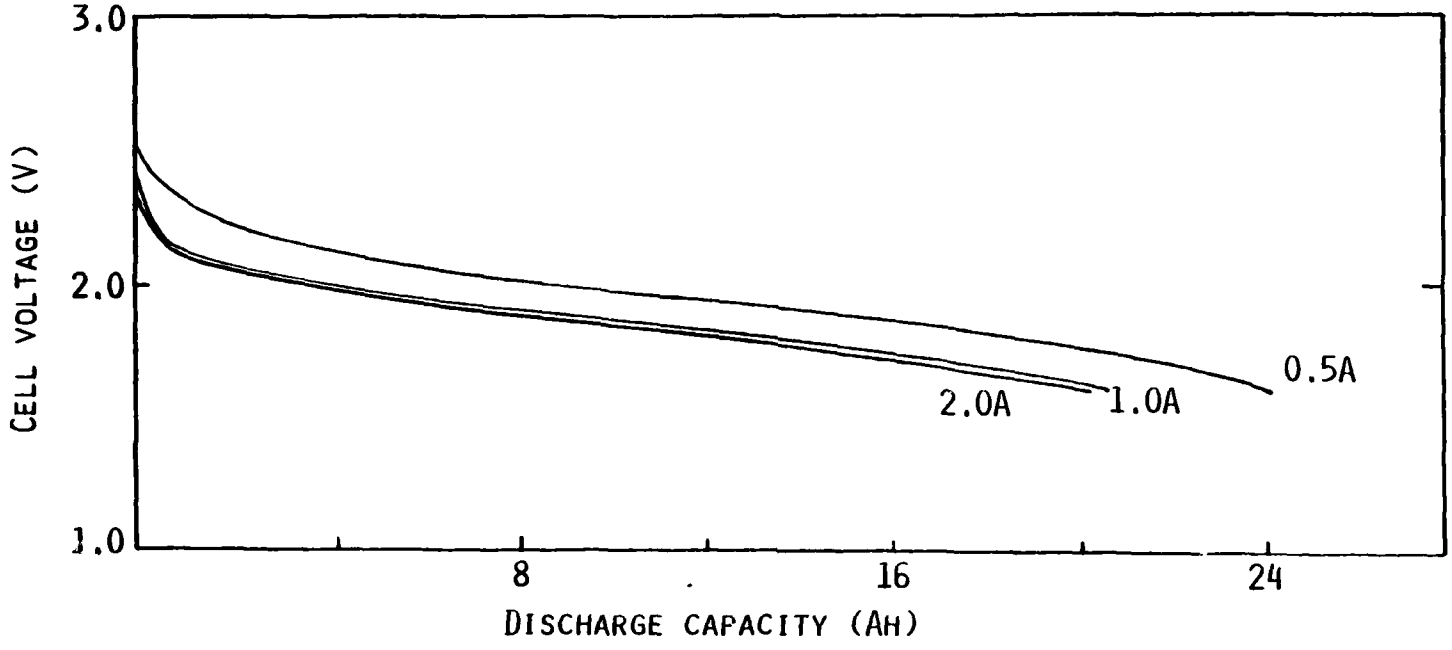

Fig. 12. Li/MoS_3 cell discharge capacity as a function of current.

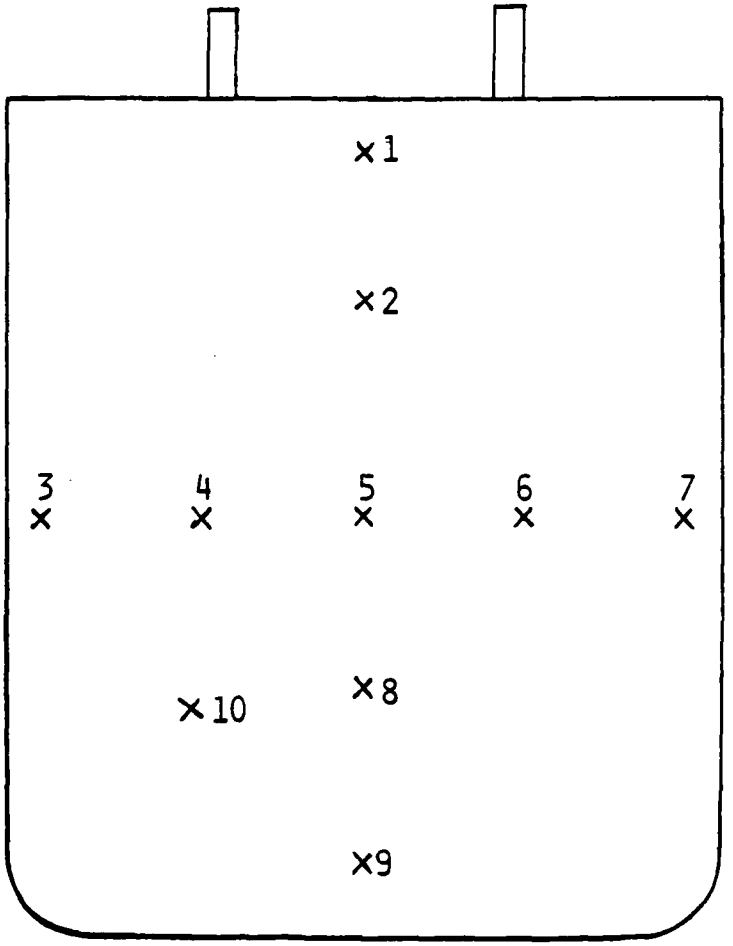

Fig. 13. Positions of cell thickness measurements.

TABLE 6

CELL 3 THICKNESS MEASUREMENTS BEFORE AND AFTER CYCLING

Position	Thickness before Cycling (inches)	Thickness after Cycling (inches)	% Increase
1	0.984	1.074	9.1
2	0.987	1.110	12.5
3	0.987	1.080	9.4
4	0.985	1.124	14.1
5	0.988	1.127	14.1
6	0.985	1.108	12.5
7	0.984	1.078	9.6
8	0.982	1.119	14.0
9	0.945	1.053	11.4
10	0.972	1.076	10.7

was $>10^5$ Ωcm. Addition of solvent (2Me-THF, distilled) to Cells 2 and 5 did not result in a recovery of electrochemical capacity. However, upon addition of fresh electrolyte solution to these cells, the internal impedance was reduced to less than 1Ω in each case suggesting that failure had occurred by loss of electrolyte salt. Electrochemical capacity was recovered in each cell; however, Cell 2 continued showing evidence of shorting. Cell 5 regained much of its original capacity (16.2 Ah on first cycle after refilling at 250 mA). Cell capacity remained, however, strongly dependent on discharge rate, e.g., at 500 mA, 10.9 Ah were obtained. This cell was subjected to 20 additional cycles before being voluntarily terminated.

3.4.3 Opening the Cells - Preliminary Observations

Cells 3, 4 and 5 were opened and the components removed for analysis after passivation of the high surface area Li with propylene carbonate. In both cells cycled over 50 cycles, large amounts of Li dendrites were found inside the anode separator bags. Some of these dendrites were seen to have grown through the Celgard bags, especially but not exclusively around the electrodes edges. Photographs of the dendrites are shown in Figure 14.

3.4.4 Electrochemical Capacity of Cathode Material

A small 20 cm^2 piece of cathode was cut from one of the cathodes removed from Cell 3. This cathode was washed several times in THF to remove propylene carbonate and placed in a small prismatic cell with fresh Li anodes and electrolyte solution. This cell was cycled briefly at 1 mA/cm^2 to determine whether the cathodes from Cell 3 retained their electrochemical capacity. The maximum capacity obtained from this electrode was approximately $0.6e^-/MoS_3$. The cell impedance was very high (~ 4Ω) and can explain the poor performance of this small cell. This experiment suggests that loss of capacity in the 20 Ah cells was accompanied by resistive film build up in the cathodes.

3.4.5 Chemical Analyses of the Cathodes

X-ray diffraction and elemental analyses were performed on cathode material from Cells 3, 4 and 5 after several washings with THF to remove any remaining $LiAsF_6$. Results of the elemental analyses are shown in Table 7. Elements not originally present in the cathode composition include Li, As, O and H. If we consider the total weight of Mo as constant in the cathode, it is apparent that the cathodes 3, 4 and 5, respectively, have gained 37.9%, 30.4% and 53.8% over their original weights. It is also apparent that cathodes from Cells 3 and 5 have lost S from their original composition.

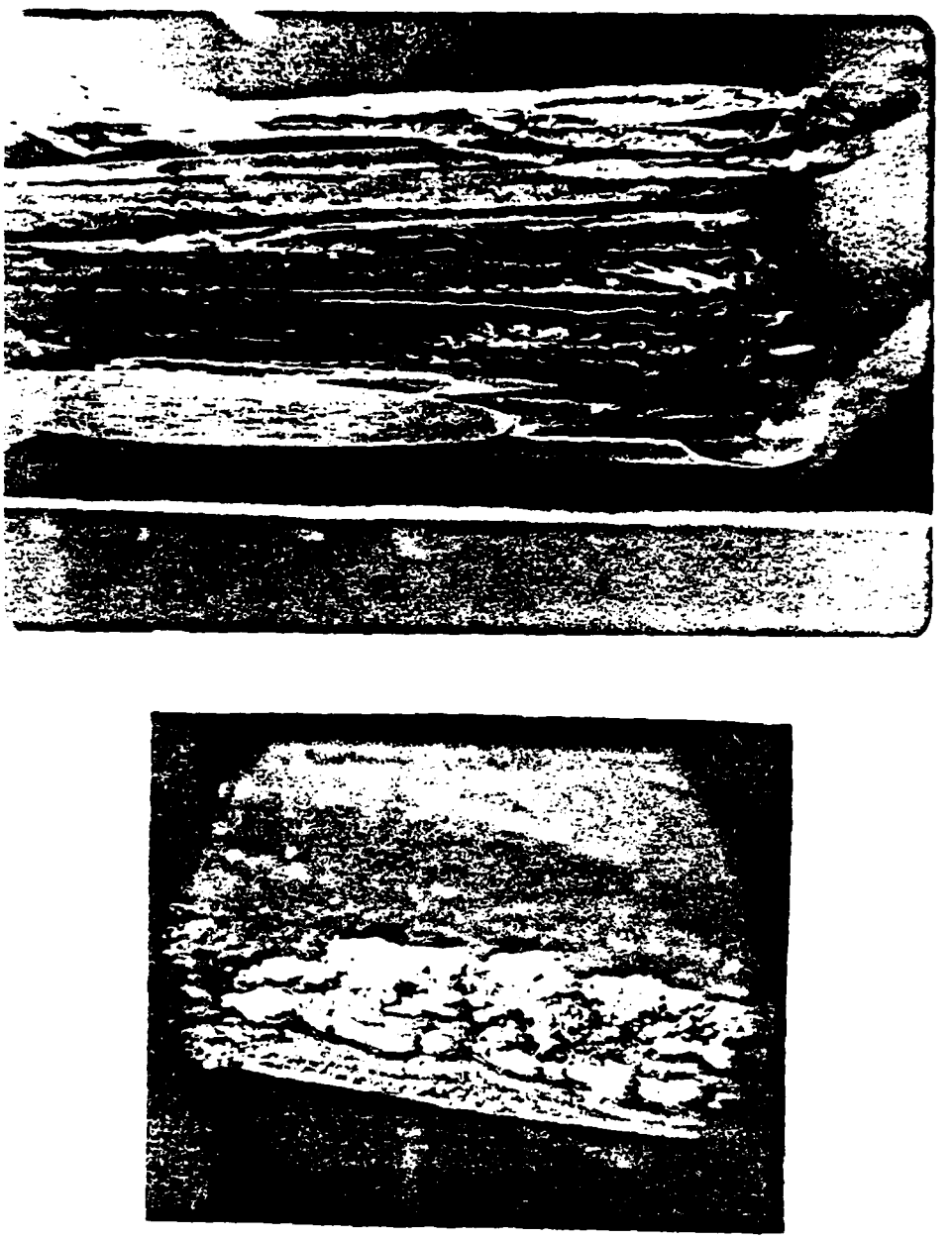

Fig. 14. Li dendrite growth in 20 Ah MoS_3 Cell 3.

Top, 2X, showing massive dendrites around edge of cell package; bottom, 20X, showing dendrite penetration through separator - rounded modules are below separator (Celgard 2400 separator is transparent).

TABLE 7

RESULTS OF ELEMENTAL ANALYSES OF CATHODES FROM CELLS 3, 4 AND 5

Element	Uncycled Cathode Material		Cell 3		Cell 4		Cell 5	
	Wt %	Mol Ratio	Wt %	Mol Ratio	Wt %	Mol Ratio	Wt %	Mol Ratio
Mo	32.46	0.34	23.54	0.25	24.90	0.26	21.11	0.22
S	32.54	1.01	20.19	0.63	25.11	0.78	20.79	0.65
C	31.20	2.60	29.28	2.50	26.50	2.18	26.47	2.21
F	3.80	0.20	6.77	0.36	7.73	0.41	9.50	0.50
Li	-	-	5.44	0.79	4.17	0.60	4.02	0.58
H	-	-	0.97	0.96	0.59	0.59	1.41	1.40
As	-	-	2.76	0.04	2.96	0.40	5.07	0.07
O	-	-	11.00	0.69	7.43	0.46	10.61	0.66
S/Mo	-	3.00	-	2.52	-	3.01	-	2.95

Results of X-ray diffraction analyses are shown in Table 8. MoS_3 itself is amorphous and shows no diffraction pattern. Both LiF and Li_2S appear to be present in the cathode from Cell 3. The major diffraction lines of Li_2S also appear in the patterns of cathodes from Cells 4 and 5. The line at 4.90 Å is attributed to Shawinigan carbon. The line at 2.67 Å in the cathode from Cell 3 has not as yet been identified.

From these analyses it is clear that chemical reactions have occurred with both the active cathode material, MoS_3, which has lost sulfur resulting in a sulfur/molybdenum stoichiometry <3, and the electrolyte salt which has lost As and Li to reaction products in the cathode. The products of these reactions are particularly evident in the cells subjected to a long cycle life. Cell 4, which was overdischarged after 20 cycles, does not show the same extent of reaction as either Cell 3 overdischarged after 50 cycles or Cell 5, cycled over 50 times without overdischarge. The amount of Li found in the cathodes is more than can be accounted for by the normal discharge reactions of the cells:

$$xLi + MoS_3 \rightarrow Li_xMoS_3,\ 0<x<3$$

The state of discharge was verified by reacting the lithiated MoS_3 with I_2 and titrating the excess I_2 with $Na_2S_2O_3$. It has not been established whether the presence of C, H and O in the cycled cathodes reflects a reaction of the solvent with the cathode material or whether their presence results from the treatment of the cycled cell with propylene carbonate to passivate the Li.

3.4.6 Chemical Analyses of the Anodes

Dendritic anode material was removed from Cells 3 and 5, washed with THF to remove $LiAsF_6$ and analyzed for elemental composition and X-ray diffraction pattern. Results of the elemental analyses are shown in Table 9, and the X-ray diffraction analyses in Table 10. Again, as in the case of the cathodes, the anodes contain reaction products from decomposition of the electrolyte salt and the cathode active material. A standard spot test utilizing KI and starch indicator in a strong HCl solution failed to detect As(V) suggesting the As is present in the As(III) state. Apparently both the As and F present in the anode are products of the reduction of $LiAsF_6$ by Li to form LiF and some As(III) compound. As in the case of the cathode material, the presence of C, H and O may result from solvent decomposition or from passivation of the highly reactive Li with propylene carbonate.

3.4.7 Cathode Decomposition Mechanism

The principal findings of the analyses of cathode and anode material are: (1) LiF and Li_2S are found in both cathode and anode, (2) MoS_3 gradually loses S during long term cycling, (3) cycling of the cells

TABLE 8

DEBYE SCHERRER POWDER DIFFRACTION PATTERNS FOR CATHODE MATERIALS
- CELLS 3, 4, AND 5 -

Li_2S		LiF		Cathode Cell 3		Cathode Cell 4		Cathode Cell 5	
d (Å)	I/I_o (%)	d (Å)	I/I_o (%)	d (Å)	I/I_o (%)	d (Å)	I/I_o (%)	d (Å)	I/I_o (%)
				4.87	30	4.92	10	4.92	20
3.30	100			3.32	100	3.34	100	3.34	100
2.86	33			2.67	30				
		2.32	95	2.31	20				
2.02	72	2.01	100	1.99	20	2.03	10	2.02	20
1.72	66								
1.65	12			1.67	10				
1.43	16	1.42	48	1.42	10				
1.31	34								
1.28	20								
		1.22	10	1.22	10				
1.17	40	1.16	11	1.15	10				
1.10	33								
1.01	18								

TABLE 9

RESULTS OF ELEMENTAL ANALYSES OF ANODES FROM CELLS 3 AND 5

Element	Anode, Cell 3		Anode, Cell 5	
	Wt %	Mol Ratio	Wt %	Mol Ratio
Li	16.81	2.42	22.43	3.23
F	22.95	1.21	9.07	0.48
S	6.08	0.19	6.36	0.20
As	16.27	0.22	17.70	0.24
O	19.95	1.25	16.34	1.02
C	14.97	1.25	5.78	0.48

TABLE 10

DEBYE SCHERRER POWDER DIFFRACTION PATTERNS FOR ANODE MATERIAL - CELLS 3 AND 5

Anode, Cell 3		Anode, Cell 5	
d (Å)	I/I_o (%)	d (Å)	I/I_o (%)
3.28	50		
		2.46	20
2.32	90	2.31	90
2.01	100	2.01	100
1.42	30	1.42	40
1.21	10		
1.16	10		

was accompanied by an increase in internal resistance caused by loss of salt in the electrolyte solution and by formation of resistive products in the cathodes. Loss of electrolyte salt can lead to formation of concentration gradients during charge and exacerbation of dendrite formation.

A possible mechanism explaining the results of the analyses described above involves the following steps: (1) MoS_3 is reduced to $MoS_{3-x} + S^{=}$, $0<x<1$, (2) $S^{=}$ is oxidized to polysulfide $S_n^{=}$, (3) Li_2S_n migrates to the anode, (4) Li_2S_n is reduced to Li_2S which precipitates, (5) $LiAsF_6$ is reduced on the surface of both anode and cathode during at least one of the previous steps. It should be emphasized that the reaction of $LiAsF_6$ is either catalyzed by the MoS_3 or coupled with a chemical reaction such as one described above. Extreme loss of electrolyte during cycling has not been observed in other secondary Li systems (e.g., $Li/LiAsF_6$ in 2Me-THF/TiS_2).

4.0 CONCLUSIONS

The following conclusions are drawn from the foregoing work:

(1) To achieve the ultimate energy density goal of 125 Wh/lb (275 Wh/kg) in a secondary Li system a cathode energy density of 290 Wh/lb (630/kg) is necessary.

(2) None of the cathode materials examined in this program, TiS_2, V_6O_{13} and MoS_3, are capable of furnishing this energy density at present. Although MoS_3 is theoretically able to provide the necessary energy, it needs more development to overcome chemical instability in the system.

(3) Life of the test cells was limited to about 50 cycles. The direct cause of failure was Li dendrite shorting which in turn was aggravated by cathode-electrolyte reactions.

TECHNICAL REPORT DISTRIBUTION LIST, GEN

	No. Copies
Office of Naval Research Attn: Code 413 800 North Quincy Street Arlington, Virginia 22217	2
ONR Pasadena Detachment Attn: Dr. R. J. Marcus 1030 East Green Street Pasadena, California 91106	1
Commander, Naval Air Systems Command Attn: Code 310C (H. Rosenwasser) Department of the Navy Washington, D.C. 20360	1
Defense Technical Information Center Building 5, Cameron Station Alexandria, Virginia 22314	12
Dr. Fred Saalfeld Chemistry Division, Code 6100 Naval Research Laboratory Washington, D.C. 20375	1
U.S. Army Research Office Attn: CRD-AA-IP P. O. Box 12211 Research Triangle Park, N.C. 27709	1
Mr. Vincent Schaper DTNSRDC Code 2803 Annapolis, Maryland 21402	1
Naval Ocean Systems Center Attn: Dr. S. Yamamoto Marine Sciences Division San Diego, California 91232	1
Naval Ocean Systems Center Attn: Mr. Joe McCartney San Diego, California 92152	1
Naval Weapons Center Attn: Dr. A. B. Amster, Chemistry Division China Lake, California 93555	1
Naval Civil Engineering Laboratory Attn: Dr. R. W. Drisko Port Hueneme, California 93401	1
Dean William Tolles Naval Postgraduate School Monterey, California 93940	1
Scientific Advisor Commandant of the Marine Corps (Code RD-1) Washington, D.C. 20380	1
Naval Ship Research and Development Center Attn: Dr. G. Bosmajian, Applied Chemistry Division Annapolis, Maryland 21401	1
Mr. John Boyle Materials Branch Naval Ship Engineering Center Philadelphia, Pennsylvania 19112	1
Mr. A. M. Anzalone Administrative Librarian PLASTEC/ARRADCOM Bldg 3401 Dover, New Jersey 07801	1

472:GAN:716-4
94/359

TECHNICAL REPORT DISTRIBUTION LIST, 359

	No. Copies
Dr. Paul Delahay Department of Chemistry New York University New York, New York 10003	1
Dr. E. Yeager Department of Chemistry Case Western Reserve University Cleveland, Ohio 41106	1
Dr. D. N. Bennion Department of Chemical Engineering Brigham Young University Provo, Utah 84602	1
Dr. R. A. Marcus Department of Chemistry California Institute of Technology Pasadena, California 91125	1
Dr. J. J. Auborn Bell Laboratories Murray Hill, New Jersey 07974	1
Dr. Adam Heller Bell Laboratories Murray Hill, New Jersey 07974	1
Dr. T. Katan Lockheed Missiles and Space Co., Inc. P. O. Box 504 Sunnyvale, California 94088	1
Dr. Joseph Singer, Code 302-1 NASA-Lewis 21000 Brookpark Road Cleveland, Ohio 44135	1
Dr. B. Brummer EIC Incorporated 55 Chapel Street Newton, Massachusetts 02158	1
Library P. R. Mallory and Company, Inc. Northwest Industrial Park Burlington, Massachusetts 01803	1
Dr. P. J. Hendra Department of Chemistry University of Southampton Southampton SO0 5NH United Kingdom	1
Dr. Sam Perone Chemistry & Materials Science Department Laurence Livermore National Lab. Livermore, California 94550	1
Dr. Royce W. Murray Department of Chemistry University of North Carolina Chapel Hill, North Carolina 27514	1
Naval Ocean Systems Center Attn: Technical Library San Diego, California 92152	1
Dr. C. E. Mueller The Electrochemistry Branch Materials Division, Research and Technology Department Naval Surface Weapons Center White Oak Laboratory Silver Spring, Maryland 20910	1
Dr. G. Goodman Johnson Controls 5757 North Green Bay Avenue Milwaukee, Wisconsin 53201	1
Dr. J. Boechler Electrochimica Corporation Attn: Technical Library 2485 Charleston Road Mountain View, California 94040	1
Dr. P. P. Schmidt Department of Chemistry Oakland University Rochester, Michigan 48063	1

472:GAN:716-4
94/359

TECHNICAL REPORT DISTRIBUTION LIST, 359

	No. Copies
Dr. H. Richtol Chemistry Department Rensselaer Polytechnic Institute Troy, New York 12181	1
Dr. A. B. Ellis Chemistry Department University of Wisconsin Madison, Wisconsin 53706	1
Dr. M. Wrighton Chemistry Department Massachusetts Institute of Technology Cambridge, Massachusetts 02139	
Larry E. Plew Naval Weapons Support Center Code 30736, Building 2906 Crane, Indiana 47522	1
S. Ruby DOE (STOR) 600 E Street Providence, Rhode Island 02192	1
Dr. Aaron Wold Brown University Department of Chemistry Providence, Rhode Island 02192	1
Dr. R. C. Chudacek McGraw-Edison Company Edison Battery Division Post Office Box 28 Bloomfield, New Jersey 07003	1
Dr. A. J. Bard University of Texas Department of Chemistry Austin, Texas 78712	1
Dr. M. M. Nicholson Electronics Research Center Rockwell International 3370 Miraloma Avenue Anaheim, California	1
Dr. R. P. Van Duyne Department of Chemistry Northwestern University Evanston, Illinois 60201	1
Dr. B. Stanley Pons Department of Chemistry University of Alberta Edmonton, Alberta CANADA T6G 2G2	1
Dr. Michael J. Weaver Department of Chemistry Michigan State University East Lansing, Michigan 48824	1
Dr. R. David Rauh EIC Corporation 55 Chapel Street Newton, Massachusetts 02158	1
Dr. J. David Margerum Research Laboratories Division Hughes Aircraft Company 3011 Malibu Canyon Road Malibu, California 90265	1
Dr. Martin Fleischmann Department of Chemistry University of Southampton Southampton 509 5NH England	1
Dr. Janet Osteryoung Department of Chemistry State University of New York at Buffalo Buffalo, New York 14214	1
Dr. R. A. Osteryoung Department of Chemistry State University of New York at Buffalo Buffalo, New York 14214	1

TECHNICAL REPORT DISTRIBUTION LIST, 359

	No. Copies
Dr. Donald W. Ernst Naval Surface Weapons Center Code R-33 White Oak Laboratory Silver Spring, Maryland 20910	1
Dr. R. Nowak Naval Research Laboratory Code 6130 Washington, D.C. 20375	1
Dr. John F. Houlihan Shenango Valley Campus Pennsylvania State University Sharon, Pennsylvania 16146	1
Dr. D. F. Shriver Department of Chemistry Northwestern University Evanston, Illinois 60201	1
Dr. D. H. Whitmore Department of Materials Science Northwestern University Evanston, Illinois 60201	1
Dr. Alan Bewick Department of Chemistry The University Southampton, S09 5NH England	1
Dr. A. Himy NAVSEA-5433 NC #4 2541 Jefferson Davis Highway Arlington, Virginia 20362	1
Dr. John Kincaid Department of the Navy Strategic Systems Project Office Room 901 Washington, D.C. 20376	1
Mr. James R. Moden Naval Underwater Systems Center Code 3632 Newport, Rhode Island 02840	1
Dr. Bernard Spielvogel U. S. Army Research Office P. O. Box 12211 Research Triangle Park, NC 27709	1
Dr. Denton Elliott Air Force Office of Scientific Research Bolling AFB Washington, D.C. 20332	1
Dr. David Aikens Chemistry Department Rensselaer Polytechnic Institute Troy, New York 12181	1
Dr. A. P. B. Lever Chemistry Department York University Downsview, Ontario M3J1P3 Canada	1
Dr. Stanislaw Szpak Naval Ocean Systems Center Code 6343 San Diego, California 95152	1
Dr. Gregory Farrington Department of Materials Science and Engineering University of Pennsylvania Philadelphia, Pennsylvania 19104	1
Dr. Bruce Dunn Department of Engineering & Applied Science University of California Los Angeles, California 90024	1

472:GAN:716-4
947359

TECHNICAL REPORT DISTRIBUTION LIST, 359

	No. Copies
M. L. Robertson Manager, Electrochemical and Power Sonices Division Naval Weapons Support Center Crane, Indiana 47522	1
Dr. Elton Cairns Energy & Environment Division Lawrence Berkeley Laboratory University of California Berkeley, California 94720	1
Dr. Micha Tomkiewicz Department of Physics Brooklyn College Brooklyn, New York 11210	1
Dr. Lesser Blum Department of Physics University of Puerto Rico Rio Piedras, Puerto Rico 00931	1
Dr. Joseph Gordon, II IBM Corporation K33/281 5600 Cottle Road San Jose, California 95193	1
Dr. Robert Somoano Jet Propulsion Laboratory California Institute of Technology Pasadena, California 91103	1
Dr. Johann A. Joebstl USA Mobility Equipment R&D Command DRDME-EC Fort Belvior, Virginia 22060	1
Dr. Judith H. Ambrus NASA Headquarters M.S. RTS-6 Washington, D.C. 20546	1
Dr. Albert R. Landgrebe U.S. Department of Energy M.S. 6B025 Forrestal Building Washington, D.C. 20595	1
Dr. T. Marks Department of Chemistry Northwestern University Evanston, Illinois 60201	1
Dr. D. Cipris Allied Corporation P. O. Box 3000R Morristown, New Jersey 07960	1
Dr. M. Philpot IBM Corporation 5600 Cottle Road San Jose, California 95193	1
Dr. Donald Sandstrom Washington State University Department of Physics Pullman, Washington 99164	1
Dr. Carl Kannewurf Northwestern University Department of Electrical Engineering and Computer Science Evanston, Illinois 60201	1
Dr. Edward Fletcher University of Minnesota Department of Mechanical Engineering Minneapolis, Minnesota 55455	1
Dr. John Fontanella U.S. Naval Academy Department of Physics Annapolis, Maryland 21402	1
Dr. Martha Greenblatt Rutgers University Department of Chemistry New Brunswick, New Jersey 08903	1
Dr. John Wassib Kings Mountain Specialties P. O. Box 1173 Kings Mountain, North Carolina 28086	1

TECHNICAL REPORT DISTRIBUTION LIST, 359

	No. Copies		No. Copies
Dr. J. J. Brophy University of Utah Department of Physics Salt Lake City, Utah 84112	1		
Dr. Walter Roth Department of Physics State University of New York Albany, New York 12222	1		
Dr. Thomas Davis National Bureau of Standards Polymer Science and Standards Division Washington, D.C. 20234	1		
Dr. Charles Martin Department of Chemistry Texas A&M University 77840	1		
Dr. Anthony Sammells Institute of Gas Technology 3424 South State Street Chicago, Illinois 60616	1		
Dr. H. Tachikawa Department of Chemistry Jackson State University Jackson, Mississippi 39217	1		
Dr. W. M. Risen Department of Chemistry Brown University Providence, Rhode Island 02192	1		


ATE
LME